Stable Adaptation in Multi-Area Load Frequency Control under Dynamically-Changing Topologies

Tao, Tian; Roy, Spandan; Baldi, Simone

DOI
10.1109/TPWRS.2020.3044436

Publication date
2021

Document Version
Accepted author manuscript

Published in
IEEE Transactions on Power Systems

Citation (APA)
Tao, T., Roy, S., & Baldi, S. (2021). Stable Adaptation in Multi-Area Load Frequency Control under Dynamically-Changing Topologies. *IEEE Transactions on Power Systems*, *36*(4), 2946-2956. https://doi.org/10.1109/TPWRS.2020.3044436

Stable Adaptation in Multi-Area Load Frequency Control under Dynamically-Changing Topologies

Tian Tao, Spandan Roy, Simone Baldi

***Abstract*—Multi-area load frequency control (LFC) selects and controls a few generators in each area of the power system in an effort to dampen inter-area frequency oscillations. To effectively dampen such oscillations, it is required to enhance and lower the control activity dynamically during operation, so as to adapt to changing circumstances. Changing circumstances should cover not only parametric uncertainties and unmodelled dynamics (e.g. aggregated area dynamics and bus dynamics), but also the increasing structural flexibility of modern power systems (e.g. protection mechanisms against faults and cyber-attacks, or topology reconfiguration mechanisms for demand response). As formal stability guarantees around such an attractive adaptive multi-area LFC concept are still lacking, this work proposes framework in which adaptation and switching are combined in a provably stable way to handle parametric uncertainty, unmodelled dynamics, and dynamical interconnections of the power system. Stability is studied in the Lyapunov theory sense using the standard structure-preserving modelling approach, and the resulting adaptive multi-area LFC design is validated using an IEEE 39-bus benchmark.**

***Index Terms*—Multi-area load frequency control, adaptive control, switching/evolving topologies, power systems**

I. Introduction

In power systems, randomness from the power load demand and from renewable energy sources may cause frequency oscillations among interconnected areas. It was recognized as an essential challenges for power system stability and security that the local (i.e. intra-area) load frequency control (LFC) should be complemented by a multi-area LFC [1] where multiple areas are connected and the frequency oscillations are balanced by adjusting the reference power of one or more governors in each area [2].

Several control methodologies have been proposed for multi-area LFC. Traditional techniques are based on fixed-gain controllers [3]–[5], which are robust when uncertainties around the nominal power system parameters (time constants, speed droops, stiffness coefficients, etc.) are small [6], [7]. In multi-area LFC, uncertainties naturally arise since the system parameters must be aggregated into equivalent time constants and coefficients, representing the dynamics at the area level [7]–[10]. The aggregation of dynamics creates the need to handle both parametric uncertainties and unmodelled dynamics, which are challenging for fixed-gain control [11]–[13]. Additionally, with the presence of renewable energy sources such as photovoltaic panels, wind farms or micro-grids, the level of uncertainty in power systems goes beyond the capabilities of fixed-gain control approaches [14]–[16], and stimulates new studies on multi-area LFC and related stability issues. Especially, "adaptive" solutions have been sought, where the controller is not fixed-gain, but capable of adapting to changing circumstances. The essential concept of adaptation in multi-area LFC is to enhance and lower the controller activity by assigning weights throughout the operation [17], [18]: adaptation ideas include having targets based on the covariances between area control errors [19], adapting participation factors [20], [21], or changing loads proportionally to frequency deviations [22].

Due to their increased flexible structure, modern power systems operate in several modes, making it impossible for a unique controller to tackle all operating conditions [14]–[16]. "Switched" controllers have been proposed as a way to handle structural changes in the system, by rapidly switching to different control configurations. Recent works where this point has been highlighted are [23], [24] (showing the need for switching among different frequency regimes), [25], [26] (showing the need for switching as per multi-agent interaction among different areas), and [27] (showing switching as the result of changing operating equilibria of the power system). For example, [19], [24], [26] show how frequency can be bounded by continuously switching among different control areas, or how switching signal can be designed, orchestrating when the load-side controller should work in the mode of frequency restoration or in the mode of load restoration. Cyber attacks provide another reason for dynamically changing topologies, [28]–[30]: as proposed countermeasures for mitigating attacks intentionally change the interconnections between areas, so as to prevent load manipulation from attackers [31]–[33].

The combination of adaptation and switching can result in a framework where the multi-area LFC control gains can change continuously to adapt to parametric uncertainty, and discontinuously to adapt to structural changes. Currently, no stable switched adaptation framework has been proposed to handle connections in power systems that change dynamically.

Control theory researchers have proposed approaches to adaptive control with switching (see [34]–[38] and references therein): however such approaches cannot find a direct application in multi-area LFC because they are either based on switching linear dynamics (whereas power flow is intrinsically nonlinear), or they require a priori bounded unmodelled dynamics (whereas aggregated area dynamics generate state-dependent uncertainty, such as bus dynamics [39]). Therefore,

This work was partially supported by Special Guiding Funds Double First-class grant 3307012001A, and Natural Science Foundation of China grant 62073074. (corresponding author: S. Baldi)

T. Tao is with Delft Center for Systems & Control, TU Delft, Delft 2628 CD, Netherlands e-mail: t.tao-1@tudelft.nl

S. Roy is with Robotics Research Centre, International Institute of Information Technology Hyderabad, India e-mail: spandan.roy@iiit.ac.in

S. Baldi is with School of Mathematics, Southeast University, Nanjing 210096, China, and guest with Delft Center for Systems & Control, TU Delft, Delft 2628 CD, Netherlands e-mail: s.baldi@tudelft.nl

despite adaptive switching control has been judged an effective framework to promote resilience, a multi-area LFC framework in which adaptation and switching are combined together in a provably stable way is still missing. Toward this goal, in this work we propose a switched adaptation framework for multi-area LFC with the following characteristics:

- A Kuramoto formulation, also called structure-preserving model, is used. This model is well known in power systems [40]–[43] to capture asynchronicity among generators in different areas. However, multi-area LFC approaches (with the exception of [24], [26]) use linear (thus less rich) versions of the structure-preserving model.
- Even compared to [24], [26], we consider the model to be affected by state-dependent uncertainty, which more appropriately captures dynamic uncertainties from aggregated area dynamics. In fact, state-dependent uncertainties cannot be bounded a priori by constants [44], [45].
- In this structure-preserving network formulation, we prove (via Lyapunov stability theory) that the proposed multi-area LFC can automatically enhance and lower the controller activity in a stable way, even in the presence of switching topologies.

The framework is tested using a benchmark IEEE 39-bus power system, divided into three areas, where all ten generators implement local LFC, but only four out of ten implement the multi-area LFC (one generator for area 1, two for area 2, one for area 3): therefore, the system presents all the uncertainties resulting from aggregating single inertia/damping terms into equivalent inertia/damping terms. Effective performance is shown, even as compared to non-adaptive strategies.

The paper is organized as follows: Sect. II introduces the system dynamics and problem formulation; The adaptive framework is in Sect. III with stability analysis in Appendix. Simulations are in Sect. IV and conclusions in Sect. V.

II. System Dynamics and Problem Formulation

Before introducing a multi-area power system and its dynamics, let us recall the standard dynamics for a single-area power system, indicated with subscript i.

A. Single-area power system

The dynamics of a single-area power system can be described as [7]–[13]:

$$T_{chi}\Delta\dot{P}_{mi}(t) = \Delta P_{\nu i}(t) - P_{mi}(t) \tag{1a}$$

$$\Delta\dot{E}_i(t) = -k_i\Delta P_{ij}(t) + k_i B_i \Delta f_i(t) \tag{1b}$$

$$T_{gi}\Delta\dot{P}_{\nu i}(t) = -\frac{\Delta f_i(t)}{R_i} - \Delta P_{\nu i}(t) - \Delta E_i(t) + u_i(t) \tag{1c}$$

$$T_{pi}\Delta\dot{f}_i(t) = -k_{pi}\Delta P_{di}(t) - k_{pi}\Delta P_{ij}(t) + k_{pi}\Delta P_{mi}(t) - \Delta f_i(t) \tag{1d}$$

$$\Delta\dot{\theta}_i(t) = \Delta f_i(t) \tag{1e}$$

where constants and variables are explained in Table I, and represent equivalent quantities, aggregated at the area level. For example, inertia, damping and time constants are equivalent time constants for the area (cf. [7]–[13] and discussion in Remark 3). Note that the proportional and integral gains in (1b) represent the gains of the local (intra-area) LFC. In (1), $\Delta P_{ij}(t)$ is a term coming from interconnection with neighboring areas (indexed by subscript j), which will be clarified in the next subsection. The symbol Δ represents the deviation from the equilibrium operating point, resulting from the solution to the power flow (or optimal power flow) equations, giving the nominal operating point of the power system [46]. The purpose of the control is to keep the network close to such equilibrium, i.e., keep $\Delta\boldsymbol{f} = [\Delta f_1, \Delta f_2, \ldots, \Delta f_n]^T$ close to 0, and $\Delta\boldsymbol{\theta} = [\Delta\theta_1, \Delta\theta_2, \ldots, \Delta\theta_n]^T$ close to $\Delta\boldsymbol{\theta}^d$, where $\Delta\boldsymbol{\theta}^d$ collects the equilibrium phase angles resulting from the power flow equations.

Table I
Nomenclature

$\Delta P_{\nu i}$	Governor valve position
ΔP_{mi}	Mechanical power output of the alternator
Δf_i	Frequency deviations
ΔE_i	Area control error signals
B_i	Proportional gains of local PI controllers
k_i	Integral gains of local PI controllers
T_{pi}	Power system time constants
k_{pi}	Power system steady-state gain
T_{gi}	Governor time constants
T_{chi}	Turbine time constants
R_i	Speed droops
T_i	Stiffness coefficients
ΔP_{di}	Load disturbances
u_i	Input signal

B. Multi-area power system

To describe the dynamics of a multi-area power network in a compact way, let us introduce some notions of graph theory.

A power system is essentially a network of dynamical systems, which are linked to each other via a *communication graph* (or *interaction graph*), that describes the allowed information flow (or the allowed physical interaction). We say that area i has an *undirected* connection to area j if the latter can receive information from (or interact with) the former and vice versa. The graph describing the connection between all areas is defined by the pair $\mathcal{G} = (\mathcal{V}, \mathcal{E})$, where $\mathcal{V} = \{1, \ldots, N\}$ is the set of nodes (areas), and $\mathcal{E} \subseteq \mathcal{V} \times \mathcal{V}$ is the set of edges (pairs of connected areas). As standard in graph theory, we assume the graph to be connected, i.e., there is a path between every pair of vertices. For a node i, let us denote with $\mathcal{N}_i$ the set of node i is connected to.

For a set of vertices, there might be different possible interconnections, or topologies. As an example, Fig. 1 shows a three-area power system where each node denotes one area, and where 4 possible connected topologies arise, indexed by $\sigma \in \Omega = [1, 2, 3, 4]$. Dynamically changing topologies can be represented by a piecewise constant time-dependent signal $\sigma(t)$, called as the *switching signal* (cf. the example in Fig. 2). To represent the evolving topologies, the following class of switching signals is considered:

Definition 1. *Average Dwell Time (ADT) [47]: For a switching signal $\sigma(t)$, let $N_\sigma(t_1, t_2)$ denote the number of discontinuities*

This article has been accepted for publication in a future issue of this journal, but has not been fully edited. Content may change prior to final publication. Citation information: DOI 10.1109/TPWRS.2020.3044436, IEEE Transactions on Power Systems

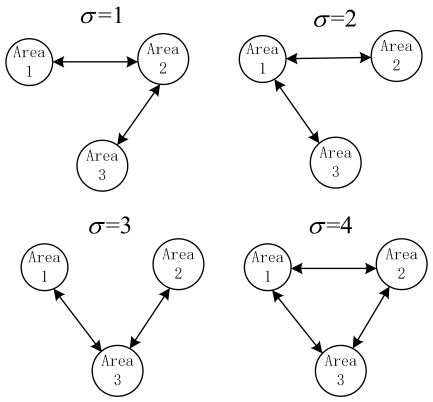

Figure 1. Example of switching topologies for a three-area power system. The switching topologies are indexed by a signal σ.

in the interval $[t_1, t_2)$. *Then* $\sigma(t)$ *has an average dwell time* ϑ *if for a given scalar* $N_0 > 0$

$$N_\sigma(t_1, t_2) \leq N_0 + (t_2 - t_1)/\vartheta, \quad \forall t_2 \geq t_1 \geq 0$$

where N_0 *is termed as chatter bound.*

Remark 1. *The class of ADT signals can represent situations in which fast switching occurs (over short intervals) as a consequence of sudden events (e.g. attacks or faults), compensated by a slower settlement phase (over long intervals).*

Interaction among two interconnected areas i and j occurs via a power flow depending on the difference between phases [41], [42]. With switching topologies, the set of neighbors of area i will be time-dependent and denoted by $\mathcal{N}_{i\sigma(t)}$. For examples, in Fig. 1, when $\sigma = 1$ node 1 has $\mathcal{N}_{11} = \{2\}$; when $\sigma = 2$, node 1 has $\mathcal{N}_{12} = \{2, 3\}$ and so on. In the following, whenever convenient, we will not explicitly write the dependence of σ on time. Then, the disturbance term ΔP_{ij} in (1d) can be defined as

$$\Delta P_{ij,\sigma}(t) = 2\pi T_i \sum_{j \in \mathcal{N}_{i\sigma}(t)} \sin(\Delta\theta_i(t) - \Delta\theta_j(t)) \tag{2}$$

$$\Delta P_{ij,\sigma}(t) = -\Delta P_{ji\sigma}(t) \tag{3}$$

If the j-th area is disconnected from the i-th area, then $\Delta P_{ij,\sigma}(t) = 0$.

C. Structure-preserving modelling

The structure-preserving (or Kuramoto) model is commonly used to analyze multi-area power systems [42], [48]. With reference to the dynamics (1)-(3), a Kuramoto-like model can be derived by assuming that the generator and turbine time constants T_{gi} and T_{chi} are much smaller than the power time constant T_{pi} (in practice T_{gi} and T_{chi} are at least 10 times smaller than T_{pi} [7]). This leads to

$$\Delta P_{mi,\sigma}(t) = -\frac{\Delta f_i(t)}{R_i} + u_{i\sigma}(t) - \Delta E_{i\sigma}(t) \tag{4a}$$

$$\Delta \dot{E}_{i\sigma}(t) = -k_i \Delta P_{ij\sigma}(t) + k_i B_i \Delta f_i(t) \tag{4b}$$

$$\Delta \dot{f}_i(t) = -\frac{k_{pi}\Delta P_{di}(t)}{T_{pi}} - \frac{k_{pi}\Delta P_{ij,\sigma}(t)}{T_{pi}} + \frac{k_{pi}\Delta P_{mi,\sigma}(t)}{T_{pi}} - \frac{\Delta f_i(t)}{T_{pi}} \tag{4c}$$

$$\Delta P_{ij,\sigma}(t) = 2\pi T_i \sum_{j \in \mathcal{N}_{i\sigma}(t)}^{N} \sin(\Delta\theta_i(t) - \Delta\theta_j(t)) \tag{4d}$$

$$\Delta \dot{\theta}_i(t) = \Delta f_i(t) \tag{4e}$$

We then obtain the following switched LFC dynamics:

$$\Delta \ddot{\theta}_i(t) = (-\frac{1}{T_{pi}} - \frac{k_{pi}}{T_{pi}R_i})\Delta\dot{\theta}_i - \frac{k_{pi}}{T_{pi}} 2\pi T_i \sum_{j \in \mathcal{N}_{i\sigma}(t)}^{N} \sin(\Delta\theta_i - \Delta\theta_j) - \frac{k_{pi}}{T_{pi}}\big(\Delta P_{di} + \Delta E_{i\sigma}(t)\big) + \frac{k_{pi}}{T_{pi}} u_{i\sigma}(t) \tag{5}$$

For compactness, system (5) is represented as

$$\Delta\ddot{\boldsymbol{\theta}}(t) = \mathbf{M}_{\sigma(t)}(\Delta\boldsymbol{\theta}(t), \Delta\dot{\boldsymbol{\theta}}(t)) + \mathbf{L}\boldsymbol{u}_\sigma(t), \ \sigma(t) \in \Omega \tag{6}$$

with $\Delta\boldsymbol{\theta} = [\Delta\theta_1, \Delta\theta_2, \ldots, \Delta\theta_n]^T$, $\boldsymbol{u}_\sigma = [u_{1\sigma}, u_{2\sigma}, \ldots, u_{n\sigma}]^T$ and with $\mathbf{L} \triangleq \text{diag}\{\frac{k_{pi}}{T_{pi}}\}$ representing the equivalent inertia of the power system. In (6), $\mathbf{M}_\sigma(\Delta\boldsymbol{\theta}(t), \Delta\dot{\boldsymbol{\theta}}(t)) \triangleq \mathbf{H}(\Delta\dot{\boldsymbol{\theta}}) + \mathbf{G}_\sigma(\Delta\boldsymbol{\theta}) + \mathbf{d}$ with

$$\mathbf{H}(\Delta\dot{\boldsymbol{\theta}}) = \text{diag}\Big\{ -\frac{1}{T_{pi}} - \frac{k_{pi}}{T_{pi}R_i}\Big\}\Delta\dot{\theta}_i \tag{7a}$$

$$\mathbf{G}_\sigma(\Delta\boldsymbol{\theta}) = \text{col}\Big\{ -\frac{k_{pi}}{T_{pi}} 2\pi T_i \sum_{j \in \mathcal{N}_{i\sigma}(t)}^{N} \sin(\Delta\theta_i - \Delta\theta_j)\Big\} \tag{7b}$$

$$\mathbf{d} = \text{col}\Big\{ -\frac{k_{pi}}{T_{pi}}\big(\Delta P_{di} + \Delta E_i\big)\Big\}, \ i = 1, \ldots, N \tag{7c}$$

where col $\{\ldots\}$ means the column vector and diag $\{\ldots\}$ is the diagonal matrix.

Based on the structure of (7), the following property holds:

Property 1. $\exists\ \overline{h}, \overline{g}_\sigma, \overline{d} \in \mathbb{R}$ *such that* $\|\mathbf{H}(\Delta\dot{\boldsymbol{\theta}})\| \leq \overline{h}\|\Delta\dot{\boldsymbol{\theta}}\|$, $\|\mathbf{G}_\sigma(\Delta\boldsymbol{\theta})\| \leq \overline{g}_\sigma$, *and* $\|\mathbf{d}(t)\| \leq \overline{d}_0 + \overline{d}_1\|\Delta\boldsymbol{\theta}\|$.

Note that the bound on $\|\mathbf{H}\|$ is proportional to $\|\Delta\dot{\boldsymbol{\theta}}\|$ thanks to the linear structure in (7a), whereas the bound on $\|\mathbf{G}\|$ is constant due to the sinusoidal a priori bounded terms in (7b). The term $\overline{d}_1$ in the disturbance arise from the phase-dependent

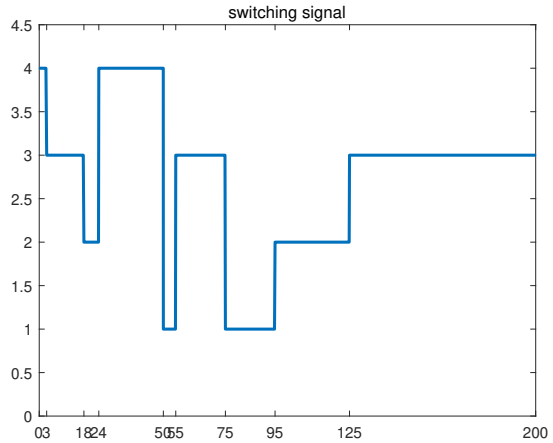

Figure 2. Switching signal representing changing topologies.

ΔE_i, evaluated by integrating (4b). It is worth mentioning that the exact values of most constants in power systems (cf. Table I) are difficult to acquire. This implies that the dynamical terms $\mathbf{H}$, $\mathbf{G}$, $\mathbf{d}$ are uncertain and their upper bounds in Property 1 are unavailable. To describe uncertainty in $\mathbf{L}$, let us decompose $\mathbf{L} = \hat{\mathbf{L}} + \Delta\mathbf{L}$ into a known (nominal) $\hat{\mathbf{L}}$ and an unknown $\Delta\mathbf{L}$. The following assumption on a priori knowledge is made:

Assumption 1. *Only nominal values (k_{pi},T_{pi}) and upper bounds ($\Delta k_{pi}, \Delta T_{pi}$) around such nominal values are available. This is described by assuming the existence of a known scalar $\bar{J}$ such that for $\mathbf{J} \triangleq \left(\mathbf{L}\hat{\mathbf{L}}^{-1} - \mathbf{I}\right)$ the following holds*

$$\|\mathbf{J}\| \leq \bar{J} < 1 \tag{8}$$

Assumption 1 is standard in inverse dynamics-based control (cf. [49]–[51]), requiring that uncertainty around the nominal $\hat{\mathbf{L}}$ is not arbitrarily large. Note that when there is no uncertainty, then $\mathbf{L} = \hat{\mathbf{L}}$ and (8) is satisfied with $\bar{J} = 0$; with more uncertainty, $\bar{J}$ tends to grow, and $\bar{J} \approx 1$ represents that $\mathbf{L} \approx 2\hat{\mathbf{L}}$ (i.e., uncertainty is around 100%). On the other hand, Assumption 1 allows arbitrarily large uncertainty in $\mathbf{H}$, $\mathbf{G}$, $\mathbf{d}$.

Let us define $\mathbf{x} \triangleq [\Delta\boldsymbol{\theta}^T \quad \Delta\dot{\boldsymbol{\theta}}^T]^T$, considered available as feedback. Using Property 1, $\mathbf{M}_\sigma(\mathbf{x})$ can be upper bounded as:

$$\|\mathbf{M}_\sigma(\mathbf{x})\| \leq \phi_{0\sigma} + \phi_{1\sigma}\|\mathbf{x}\|, \tag{9}$$

where $\phi_{0\sigma} = \overline{g}_\sigma + \overline{d}, \phi_{1\sigma} = \overline{h} + \overline{d}_1$ (the subscript in $\phi_{1\sigma}$ is used for consistency in notation) are derived from (7), and are finite but *unknown scalars* according to Assumption 1.

The notion of Uniform Ultimate Boundedness is the standard stability concept in robust adaptive control (cf. [45, Def. 3] or [52, Def. 3.4.12] for details).

Definition 2. ***(Uniform Ultimate Boundedness (UUB))*** *The switched system (6) under switching signal $\sigma(\cdot)$ is uniformly ultimately bounded if there exists a convex and compact set $\mathcal{C}$ such that for every initial condition $x(0) = x_0$, there exists a finite time $T(x_0)$ such that $x(t) \in \mathcal{C}$ for all $t \geq T(x_0)$.*

This leads to the LFC problem formulation:

Problem Formulation. *Under Assumption 1, the aim is to design an adaptive multi-area LFC controller $\boldsymbol{u}_\sigma$ such that can track (in the sense of UUB) a desired constant frequency $\Delta\dot{\boldsymbol{\theta}}^d = \mathbf{0}$ under uncertainty and ADT switching topologies.*

The following remarks clarify the distinguishing features and innovations of the proposed problem formulation.

Remark 2. *Compared to conventional multi-area LFC dynamics, where the linearized power flow $(\Delta\theta_i - \Delta\theta_j)$ is used, which is valid only for small phases [7]–[13], we consider the nonlinear power flow $\sin(\Delta\theta_i - \Delta\theta_j)$. This makes the dynamics more rich and the control design more challenging and open in literature.*

Remark 3. *The upper bound structure in* (9) *is state-dependent. In multi-area LFC, state-dependent uncertainties naturally arise since the system parameters must be aggregated into equivalent time constants and coefficients, representing the dynamics at the area level [7]–[10]. Bus dynamics are also state-dependent uncertainties according to the structure-preserving model [39]. The aggregation of dynamics creates the need to handle both parametric uncertainties and state-dependent unmodelled dynamics [11]–[13].*

Table II
CONTROL VARIABLES AND PARAMETERS

$\mathbf{r}_\sigma$	tracking error variable
$\mathbf{K}_{1\sigma}$	linear proportional gain
$\mathbf{K}_{2\sigma}$	linear derivative gain
$\hat{\boldsymbol{L}}$	nominal inertia
ϵ	anti-chattering constant
ω	ultimate bound parameter
ρ_σ	overall robust adaptive gain
$\hat{\phi}_{ip},\ \hat{\phi}_{i\overline{p}}$	adaptive gains (active and inactive topologies)
$\gamma_{ip},\ \gamma_{i\overline{p}}$	auxiliary gains (active and inactive topologies)
α_i	leakage rate of adaptive gains $\hat{\phi}_{ip},\ \hat{\phi}_{i\overline{p}}$
β_i	leakage rate of auxiliary gain $\gamma_{ip},\ \gamma_{i\overline{p}}$
ν_{ip}	nonlinear leakage of auxiliary gains $\gamma_{ip},\ \gamma_{i\overline{p}}$
$\bar{J}$	maximum uncertainty in $\mathbf{L}$

III. STABLE ADAPTIVE LFC DESIGN AND ANALYSIS

Let $\boldsymbol{e}(t) \triangleq \Delta\boldsymbol{\theta}(t) - \Delta\boldsymbol{\theta}^d(t)$ and $\boldsymbol{\xi}(t) \triangleq [\boldsymbol{e}(t)^T \ \dot{\boldsymbol{e}}(t)^T]^T$. A summary of the control variables and parameters in this section can be found in Table II. Define a tracking error variable

$$\mathbf{r}_\sigma \triangleq \mathbf{B}^T\mathbf{P}_\sigma\boldsymbol{\xi}, \qquad \sigma \in \Omega \tag{10}$$

where $\mathbf{P}_\sigma > \mathbf{0}$ is the solution to the Lyapunov equation

$$\mathbf{A}_\sigma^T\mathbf{P}_\sigma + \mathbf{P}_\sigma\mathbf{A}_\sigma = -\mathbf{Q}_\sigma \tag{11}$$

for some $\mathbf{Q}_\sigma > \mathbf{0}$ are the user-defined parameters, $\mathbf{A}_\sigma \triangleq \begin{bmatrix} \mathbf{0} & \mathbf{I} \\ -\mathbf{K}_{1\sigma} & -\mathbf{K}_{2\sigma} \end{bmatrix}$ and $\mathbf{B} \triangleq \begin{bmatrix} \mathbf{0} & \mathbf{I} \end{bmatrix}^T$. Here, $\mathbf{K}_{1\sigma}$ and $\mathbf{K}_{2\sigma}$ are two user-defined positive definite gain matrices and their positive definiteness guarantees $\mathbf{A}_\sigma$ to be Hurwitz.

The switched multi-area LFC is designed as

$$\boldsymbol{u}_\sigma = \hat{\mathbf{L}}^{-1}(-\mathbf{K}_{1\sigma}\boldsymbol{e} - \mathbf{K}_{2\sigma}\dot{\boldsymbol{e}} - \Delta\boldsymbol{u}_\sigma), \tag{12a}$$

$$\Delta\boldsymbol{u}_\sigma = \omega\rho_\sigma\frac{\boldsymbol{r}_\sigma}{\sqrt{\|\boldsymbol{r}_\sigma\|^2 + \epsilon}}, \tag{12b}$$

with $\epsilon > 0$ a small scalar to avoid control chatter and $\omega > 1$ a user-defined scalar affecting the ultimate bound. The design of ρ_σ is discussed later. Substituting (12a) in (6) yields

$$\begin{aligned}\ddot{\boldsymbol{e}} = \Delta\ddot{\boldsymbol{\theta}} &= \mathbf{M}_\sigma + \mathbf{L}\boldsymbol{u}_\sigma \\ &= \mathbf{M}_\sigma + \left(\mathbf{L}\hat{\mathbf{L}}^{-1} - \mathbf{I}\right)(-\mathbf{K}_{1\sigma}\boldsymbol{e} - \mathbf{K}_{2\sigma}\dot{\boldsymbol{e}} - \Delta\boldsymbol{u}_\sigma) \\ &\quad + (-\mathbf{K}_{1\sigma}\boldsymbol{e} - \mathbf{K}_{2\sigma}\dot{\boldsymbol{e}} - \Delta\boldsymbol{u}_\sigma) \\ &= -\mathbf{K}_{1\sigma}\boldsymbol{e} - \mathbf{K}_{2\sigma}\dot{\boldsymbol{e}} - (\mathbf{I} + \mathbf{J})\Delta\boldsymbol{u}_\sigma + \boldsymbol{\Psi}_\sigma,\end{aligned} \tag{13}$$

where $\boldsymbol{\Psi}_\sigma \triangleq \mathbf{M}_\sigma - \mathbf{J}(\mathbf{K}_{1\sigma}\boldsymbol{e} + \mathbf{K}_{2\sigma}\dot{\boldsymbol{e}})$ is treated as the overall uncertainty. Hence, using Assumptions 1, one can verify the existence of $\phi^*_{i\sigma} \in \mathbb{R}^+ \ i = 0, 1$ such that for all $\sigma \in \Omega$

$$\|\boldsymbol{\Psi}_\sigma\| \leq \phi^*_{0\sigma} + \phi^*_{1\sigma}\|\boldsymbol{\xi}\|, \tag{14}$$

where $\phi^*_{0\sigma} = \phi_{0\sigma} + \phi_{1\sigma}||x^d||$, $\phi^*_{1\sigma} = \phi_{1\sigma} + \|\mathbf{J}\|\|\mathbf{K}_{1\sigma}\mathbf{K}_{2\sigma}\|$ (based on the fact of $\mathbf{x} = \Delta\boldsymbol{\theta}^d + \boldsymbol{\xi}$) are unknown finite scalars. After defining the structures of the upper bound of $\|\boldsymbol{\Psi}_\sigma\|$ in (14), the gain ρ_σ in (12b) is proposed as

$$\rho_\sigma = \frac{1}{1 - \bar{J}}\left\{(\hat{\phi}_{0\sigma} + \gamma_{0\sigma}) + (\hat{\phi}_{1\sigma} + \gamma_{1\sigma})\|\boldsymbol{\xi}\|\right\} \tag{15}$$

where $\hat{\phi}_{0\sigma}$, $\hat{\phi}_{1\sigma}$ are the estimates of the upper bounds $\phi^*_{0\sigma}, \phi^*_{1\sigma}$, and $\gamma_{0\sigma}$, $\gamma_{1\sigma}$ are auxiliary gains.

The main idea of switching structure (12) is that a different control action is activated depending on the active topology. Let p denote the index of the active topology for $t \in [t_l\ t_{l+1})$, $\mathcal{I}(p)$ denote the set of inactive topologies. The gains in (15) are evaluated using the following laws:

$$\dot{\hat{\phi}}_{ip} = \|\mathbf{r}_p\|\|\boldsymbol{\xi}\|^i - \alpha_{ip}\hat{\phi}_{ip}, \quad \dot{\gamma}_{ip} = 0, \tag{16a}$$

$$\dot{\hat{\phi}}_{i\overline{p}} = 0, \quad \dot{\gamma}_{i\overline{p}} = -\left(\beta_{i\overline{p}} + \overline{\nu}_{i\overline{p}}\hat{\phi}^4_{i\overline{p}}\right)\gamma_{i\overline{p}} + \beta_{i\overline{p}}\nu_{i\overline{p}}, \tag{16b}$$

$$\text{with } \hat{\phi}_{ip}(0) > 0,\ \gamma_{i\overline{p}}(0) > \nu_{i\overline{p}}, \tag{16c}$$

$$\alpha_{ip} > \zeta_p/2, \beta_{i\overline{p}} > \zeta_{\overline{p}}/2. \tag{16d}$$

where $\overline{p} \in \mathcal{I}(p)$; $\alpha_{ip}, \beta_{i\overline{p}}, \nu_{i\overline{p}}, \overline{\nu}_{i\overline{p}} \in \mathbb{R}^+$, $i = 0, 1$ are static design scalars. Note that $\hat{\phi}_{i\sigma}$ is only updated for the active topology p, while the gain $\gamma_{i\sigma}$ is updated only for inactive topologies $\overline{p}$. The first term in $\dot{\hat{\phi}}_{ip}$ adjusts the gain according to the current error, whereas the second term in $\dot{\hat{\phi}}_{ip}$ and the first term in $\dot{\gamma}_{i\overline{p}}$ are stabilizing leakage factors (cf. the derivations in Appendix (24), (28), (31)-(32)).

Using the framework of ADT, we can define the set of dynamically-changing topology variations that can be tolerated by controller (12), (15), (16) without losing stability. To this purpose, let us define $\bar{\zeta}_M \triangleq \max_{p\in\Omega} \lambda_{\max}(\mathbf{P}_p)$ and $\underline{\zeta}_m \triangleq \min_{p\in\Omega} \lambda_{\min}(\mathbf{P}_p)$. Following **Definition 1** of ADT, the switching law condition to guarantee stability is proposed as

$$\vartheta > \ln \mu/\kappa, \tag{17}$$

where $\mu \triangleq \bar{\zeta}_M/\underline{\zeta}_m \geq 1$; κ is a scalar defined as $0 < \kappa < \zeta$ where $\zeta_p \triangleq (\lambda_{\min}(\mathbf{Q}_p)/\lambda_{\max}(\mathbf{P}_p))$ and $\zeta \triangleq \min_{p\in\Omega}\{\zeta_p\}$.

Table II explains the meaning of control variables and parameters and Algorithm 1 summarizes the design steps to be followed to implement the proposed adaptive control framework. The following stability result is given in the context of Lyapunov theory [52], while the proof in the Appendix clarifies how the design (12), (15), (16) and (17) was obtained.

Theorem 1. *Under Property 1 and Assumption 1, the closed-loop trajectories (including the tracking error) of power system (6) employing multi-area LFC (12) and (15) with adaptive law (16) and ADT switching law (17) are UUB.*

Proof. See Appendix. □

IV. IEEE 39 BUS TEST CASE

The effectiveness of the proposed LFC design is tested using the IEEE 39 bus system [13]. To implement the multi-area LFC, the system is divided into three areas (cf. Fig. 3). Tie lines between buses 2 and 3, and buses 17 and 27 connect areas 1 and 2; tie lines between buses 5 and 8, and buses 7 and 8 connect areas 2 and 3, and a tie line between buses 1 and 2 connects areas 1 and 3. While all ten generators are equipped with a local LFC, only a few (four) generators implement the multi-area LFC to dampen oscillation among areas: the generator connected to bus 37 is responsible for multi-area LFC in area 1; the generators connected to buses 32 and 36 are responsible in equal percentage for multi-area LFC in area 2; the generator connected to bus 39 is responsible for multi-area LFC in area 3. This setting is consistent with [13].

Algorithm 1 Design and implementation steps of the proposed multi-area LFC

Design Step 1: with $\Delta\dot{\boldsymbol{\theta}}^d = 0$, obtain the desired phase $\Delta\boldsymbol{\theta}^d$ from power flow equations at the nominal operating point;
Design Step 2: define the tracking error variable as in (10) via the Lyapunov equation (11);
Design Step 3: compute the control law $\boldsymbol{u}_\sigma$ as in (12) and (15) with suitable $\mathbf{K}_{1\sigma}$, $\mathbf{K}_{2\sigma}$ and ω, ε;
Design Step 4: design the adaptive laws as in (16);
Design Step 5: design the switching law as in (17).

Implementation Step 1: for each area i, assign one or more generators for multi-area LFC; use the inertia of those generators (or their average) to obtain the nominal $\hat{\mathbf{L}}$ in (12a);
Implementation Step 2: write $\boldsymbol{u}_\sigma = [u_{1\sigma}, u_{2\sigma}, \ldots, u_{n\sigma}]^T$, where $u_{i\sigma}$ is the control assigned to area i;
Implementation Step 3: if only one generator is assigned for multi-area LFC in area i, assign $u_{i\sigma}$ to that generator; if more generators are assigned for multi-area LFC in area i, partition $u_{i\sigma}$ among those generators (e.g. in equal proportions).

A. Design and considerations on control disaggregation

Each generator responsible for multi-area LFC in one area "sees" the area an aggregated dynamical system (where the aggregated dynamics also include the local LFC dynamics and the bus dynamics). The actual parameters of such aggregated dynamical system are mostly unknown and not available for control design and, in view of Assumption 1, the only available knowledge for control design are the inertia parameters of the generators (cf. Table III). In our test case, only inertia of generator 37, the average inertia of generator 32 and 36, and the inertia of generator 39 are used to obtain the nominal $\hat{\mathbf{L}}$ in (12a), according to Algorithm 1.

The solutions to the Lyapunov equations are

$$\mathbf{P}_1 = \begin{bmatrix} 35.0728 & 0 & 0 & 0.2581 & 0 & 0 \\ 0 & 35.0728 & 0 & 0 & 0.2581 & 0 \\ 0 & 0 & 35.0728 & 0 & 0 & 0.2581 \\ 0.2581 & 0 & 0 & 2.0564 & 0 & 0 \\ 0 & 0.2581 & 0 & 0 & 2.0564 & 0 \\ 0 & 0 & 0.2581 & 0 & 0 & 2.0564 \end{bmatrix}$$

$$\mathbf{P}_2 = \begin{bmatrix} 32.2954 & 0 & 0 & 0.4753 & 0 & 0 \\ 0 & 32.2954 & 0 & 0 & 0.4753 & 0 \\ 0 & 0 & 32.2954 & 0 & 0 & 0.4753 \\ 0.4753 & 0 & 0 & 1.8929 & 0 & 0 \\ 0 & 0.4753 & 0 & 0 & 1.8929 & 0 \\ 0 & 0 & 0.4753 & 0 & 0 & 1.8929 \end{bmatrix}$$

$$\mathbf{P}_3 = \begin{bmatrix} 48.3565 & 0 & 0 & 0.5694 & 0 & 0 \\ 0 & 48.3565 & 0 & 0 & 0.5694 & 0 \\ 0 & 0 & 48.3565 & 0 & 0 & 0.5694 \\ 0.5694 & 0 & 0 & 2.8334 & 0 & 0 \\ 0 & 0.5694 & 0 & 0 & 2.8334 & 0 \\ 0 & 0 & 0.5694 & 0 & 0 & 2.8334 \end{bmatrix}$$

$$\mathbf{P}_4 = \begin{bmatrix} 48.5521 & 0 & 0 & 0.8575 & 0 & 0 \\ 0 & 97.1043 & 0 & 0 & 0.8575 & 0 \\ 0 & 0 & 97.1043 & 0 & 0 & 0.8575 \\ 0.8575 & 0 & 0 & 2.8483 & 0 & 0 \\ 0 & 0.8575 & 0 & 0 & 2.8483 & 0 \\ 0 & 0 & 0.8575 & 0 & 0 & 2.8483 \end{bmatrix}$$

This article has been accepted for publication in a future issue of this journal, but has not been fully edited. Content may change prior to final publication. Citation information: DOI 10.1109/TPWRS.2020.3044436, IEEE Transactions on Power Systems

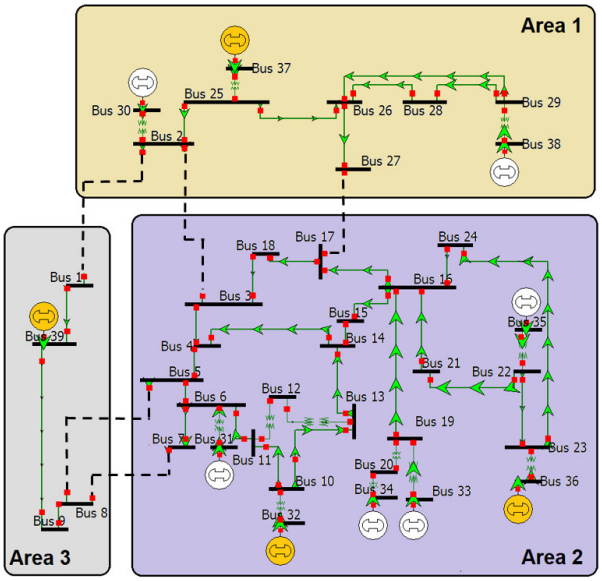

Figure 3. Benchmark IEEE 39-bus system divided into three areas. All ten generators implement local (intra-area) LFC, while four generators (indicated in yellow) additionally implement multi-area LFC.

Table III
INERTIA OF GENERATORS IN IEEE 39-BUS SYSTEM.

0.2653	Inertia of Generator 30
0.1607	Inertia of Generator 31
0.1899	Inertia of Generator 32
0.1517	Inertia of Generator 33
0.1379	Inertia of Generator 34
0.1846	Inertia of Generator 35
0.1401	Inertia of Generator 36
0.1289	Inertia of Generator 37
0.1830	Inertia of Generator 38
0.2228	Inertia of Generator 39

We further select $\mathbf{K}_{1\sigma} = 15\mathbf{I}$, $\mathbf{K}_{2\sigma} = 0.8\mathbf{I}$, same for every topology. The Lyapunov matrices yield $\zeta = 0.2059$, $\mu = 25.7588$, and, when $\kappa = 0.9\zeta$, the ADT $\ln \mu/\kappa = 17.5316$, according to (17). This implies that topology can switch up to every 17.5 seconds on average. The switching law $\sigma(t)$ previously presented in Fig. 2 is adopted in simulations.

Control design parameters are selected as: $\epsilon = 0.1, \omega = 2$, $\bar{J} = 0.3$, $\alpha_{ip} = 0.2$, $\beta_{i\bar{p}} = 0.15$, $\bar{\nu}_{i\bar{p}} = 1$, $\nu_{i\bar{p}} = 0.7$ with $i = 0, 1$. The initial gains are $\hat{\phi}_{0p}(0) = 0.3$, $\gamma_{i\bar{p}}(0) = 25$.

B. Simulation Results and Discussion

To compare and assess the benefits of the proposed multi-area LFC approach, we implement the local LFC (without multi-area LFC), and a standard non-adaptive multi-area LFC, which is a proportional derivative controller with proportional gain equal to 3 and derivative gain equal to 30 (such gains have been tuned to provide the best performance).

The performance of the three approaches (only local LFC, non-adaptive multi-area LFC and adaptive multi-area LFC) are reported in Table IV in terms of norm of phase deviations and norm of frequency deviations. Because synchronization of a power system to a constant frequency implies a rotation with linearly increasing phase (being phase the integral of frequency), we use bus 9 as a rotating reference [53]. By this, we can evaluate the frequency deviation, and compare the phase deviation with the desired equilibrium phase resulting from the solution to the optimal power flow. The percentage improvements in Table IV show that the proposed adaptive multi-area LFC outperforms the non-adaptive multi-area LFC almost six times in terms of phase deviations (-3.05% vs -17.73%) and almost three times in terms of frequency deviations (-20.45% vs -60.22%). This implies reduced frequency oscillations and smallest deviations from the optimal power flow phase. The evolution of phase deviations and frequency deviations are reported in Fig. 4 for the local LFC, in Fig. 5 for the non-adaptive multi-area LFC and in Fig. 6 for the proposed adaptive multi-area LFC. In these figures, all phase deviations are bounded, transients occur due to topology changes at the switching instants in Fig. 2, and the size of the oscillations are also influenced by the generator parameters and the load.

Finally, Fig. 7 and Fig. 8 illustrate the adaptive gains for active and inactive topologies ($\hat{\phi}_{ip}$, $\hat{\phi}_{i\bar{p}}$, γ_{ip} and $\gamma_{i\bar{p}}$, $i = 0, 1$). The gains $\hat{\phi}_{i\bar{p}}$ remain constant when the corresponding topology is inactive, while the gains $\hat{\phi}_{ip}$ adapt when the corresponding topology is activated. On the other hand, the gains $\gamma_{i\bar{p}}$ adapt when the corresponding topology is inactive, while the gains γ_{ip} remain constant when the corresponding topology is activated. Therefore, all gains automatically adapt or remain constant in order to obtain stability for any topology. This shows the adaptation capabilities of the proposed framework.

V. CONCLUSION

This paper proposed a switched adaptation framework for multi-area LFC based on nonlinear structure-preserving (Kuramoto) dynamics with state-dependent uncertainty. In this modelling framework, which provides a more rich description of uncertainties typically considered in multi-area LFC, stable self-reconfiguration was proven using Lyapunov theory in the presence of changing topologies among multi-area power systems. Interesting future work is to extend the proposed methodology for wide-area damping control, which requires a modelling approach beyond the structure-preserving model.

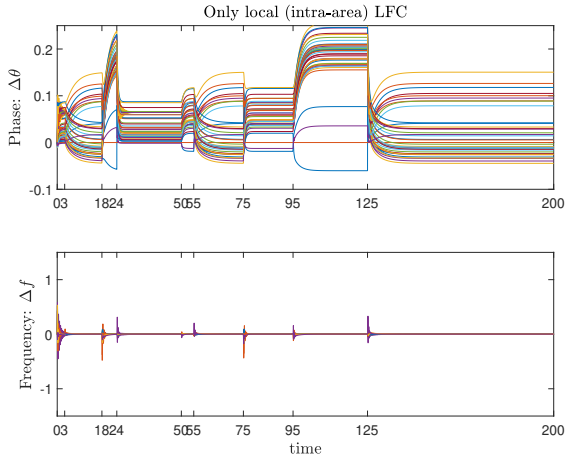

Figure 4. Phase and frequency deviations for all nodes with only local (intra-area) LFC (no multi-area LFC).

This article has been accepted for publication in a future issue of this journal, but has not been fully edited. Content may change prior to final publication. Citation information: DOI 10.1109/TPWRS.2020.3044436, IEEE Transactions on Power Systems

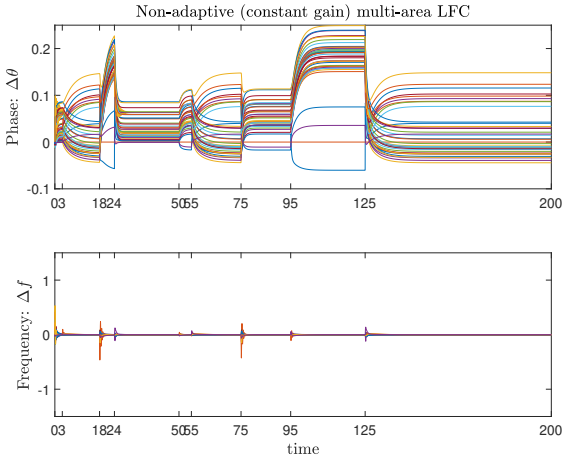

Figure 5. Phase and frequency deviations for all nodes with local (intra-area) LFC and non-adaptive (constant gain) multi-area LFC.

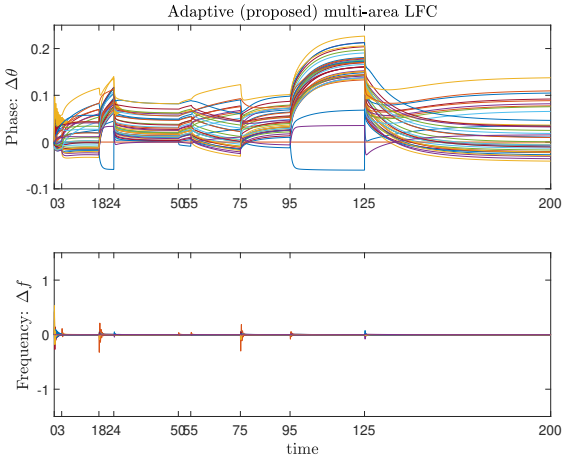

Figure 6. Phase and frequency deviations for all nodes with local (intra-area) LFC and adaptive (proposed) multi-area LFC.

Table IV
ERROR DEVIATION NORMS FOR NON-ADAPTIVE AND ADAPTIVE MULTI-AREA LFC, WITH IMPROVEMENTS REPORTED AS COMPARED TO THE ONLY-LOCAL LFC SCENARIO (WITHOUT MULTI-AREA LFC).

	Norm of Phase Deviation	Norm of Frequency Deviation
Only-Local LFC	226.06 (-)	85.35 (-)
Non-adaptive Multi-area LFC	219.35 **(-3.05%)**	70.86 **(-20.45%)**
Adaptive (proposed) Multi-area	192.01 **(-17.73%)**	53.27 **(-60.22%)**

APPENDIX
PROOF OF THEOREM 1

Stability is analyzed using the Lyapunov function

$$V(t) = \frac{1}{2}\boldsymbol{\xi}^T(t)\mathbf{P}_{\sigma(t)}\boldsymbol{\xi}(t) + \frac{1}{2}\sum_{p=1}^{N}\sum_{i=0}^{1}\{(\hat{\phi}_{ip}(t) - \phi^*_{ip})^2 + \gamma^2_{ip}(t)\}, \tag{18}$$

The following error dynamics is obtained from (13)

$$\dot{\boldsymbol{\xi}} = \mathbf{A}_\sigma\boldsymbol{\xi} + \mathbf{B}\big(\boldsymbol{\Psi}_\sigma - (\mathbf{I}+\mathbf{J})\Delta\boldsymbol{u}_\sigma\big) \tag{19}$$

We first investigate the behavior of $V(t)$ at the switching instants. Let subsystem $\sigma(t^-_{l+1})$ be active when $t \in [t_l \quad t_{l+1})$ and subsystem $\sigma(t_{l+1})$ is active when $t \in [t_{l+1} \quad t_{l+2})$. At the switching instant t_{l+1}, we have before switching

$$V(t^-_{l+1}) = \frac{1}{2}\boldsymbol{\xi}^T(t^-_{l+1})\mathbf{P}_{\sigma(t^-_{l+1})}\boldsymbol{\xi}(t^-_{l+1}) + \frac{1}{2}\sum_{p=1}^{N}\sum_{i=0}^{1}\{(\hat{\phi}_{ip}(t^-_{l+1}) - \phi^*_{ip})^2 + \gamma^2_{ip}(t^-_{l+1})\},$$

and after switching

$$V(t_{l+1}) = \frac{1}{2}\boldsymbol{\xi}^T(t_{l+1})\mathbf{P}_{\sigma(t_{l+1})}\boldsymbol{\xi}(t_{l+1}) + \frac{1}{2}\sum_{p=1}^{N}\sum_{i=0}^{1}\{(\hat{\phi}_{ip}(t_{l+1}) - \phi^*_{ip})^2 + \gamma^2_{ip}(t_{l+1})\}.$$

In accordance with the continuity of the tracking error $\boldsymbol{\xi}$ in (19) and of the gains $\hat{\phi}_{i\sigma}$'s and $\gamma_{i\sigma}$ in (16), we have $\boldsymbol{\xi}(t^-_{l+1}) = \boldsymbol{\xi}(t_{l+1})$, $(\hat{\phi}_{ip}(t^-_{l+1}) - \phi^*_{ip}) = (\hat{\phi}_{ip}(t_{l+1}) - \phi^*_{ip})$ and $\gamma_{ip}(t^-_{l+1}) = \gamma_{ip}(t_{l+1})$. Further, owing to the facts $\boldsymbol{\xi}^T(t)\mathbf{P}_{\sigma(t)}\boldsymbol{\xi}(t) \leq \bar{\zeta}_M\boldsymbol{\xi}^T(t)\boldsymbol{\xi}(t)$ and $\boldsymbol{\xi}^T(t)\mathbf{P}_{\sigma(t)}\boldsymbol{\xi}(t) \geq \underline{\zeta}_m\boldsymbol{\xi}^T(t)\boldsymbol{\xi}(t)$, one has

$$V(t_{l+1}) - V(t^-_{l+1}) \leq \frac{\bar{\zeta}_M - \underline{\zeta}_m}{2\underline{\zeta}_m}\boldsymbol{\xi}^T(t_{l+1})\mathbf{P}_{\sigma(t^-_{l+1})}\boldsymbol{\xi}(t_{l+1}) \leq \frac{\bar{\zeta}_M - \underline{\zeta}_m}{\underline{\zeta}_m}V(t^-_{l+1}) \qquad \Rightarrow V(t_{l+1}) \leq \mu V(t^-_{l+1}), \tag{20}$$

The behavior of $V(t)$ between two consecutive switching instants, i.e., when $t \in [t_l \quad t_{l+1})$ is studied subsequently. Without the loss of generality, the closed-loop stability is analyzed by taking $p = \sigma(t^-_{l+1})$ as an active system.

Using (10), (19) and the Lyapunov equation $\mathbf{A}^T_\sigma\mathbf{P}_\sigma + \mathbf{P}_\sigma\mathbf{A}_\sigma = -\mathbf{Q}_\sigma$, the time derivative of (18) yields

$$\dot{V}(t) \leq -\frac{1}{2}\boldsymbol{\xi}^T(t)\mathbf{Q}_{\sigma(t^-_{l+1})}\boldsymbol{\xi}(t) + \|\boldsymbol{\Psi}_{\sigma(t^-_{l+1})}\|\|\mathbf{r}_{\sigma(t^-_{l+1})}\| - (1-\bar{J})\rho_{\sigma(t^-_{l+1})}\omega\frac{\|\mathbf{r}_{\sigma(t^-_{l+1})}\|^2}{\sqrt{\|\mathbf{r}_{\sigma(t^-_{l+1})}\|^2 + \epsilon}} + \sum_{p=1}^{N}\sum_{i=0}^{1}\Big\{(\hat{\phi}_{ip}(t) - \phi^*_{ip})\dot{\hat{\phi}}_{ip}(t) + \gamma_{ip}(t)\dot{\gamma}_{ip}(t)\Big\}. \tag{21}$$

For the ease of analysis, we define a region such that

$$\omega\frac{\|\mathbf{r}_\sigma\|^2}{\sqrt{\|\mathbf{r}_\sigma\|^2 + \epsilon}} \geq \|\mathbf{r}_\sigma\| \Rightarrow \|\mathbf{r}_\sigma\| \geq \sqrt{\frac{\epsilon}{\omega^2 - 1}} \triangleq \varphi. \tag{22}$$

with $\omega > 1$ a user defined scalar. We analyse the behavior of the Lyapunov function for the two scenarios:

S1: $\|\mathbf{r}_\sigma\| \geq \varphi$ and S2: $\|\mathbf{r}_\sigma\| < \varphi$.

Scenario $S1$**:** It can be observed from the adaptive law (16) that the gains $\hat{\phi}_{i\overline{p}}$ and γ_{ip} remain constant during inactive and

This article has been accepted for publication in a future issue of this journal, but has not been fully edited. Content may change prior to final publication. Citation information: DOI 10.1109/TPWRS.2020.3044436, IEEE Transactions on Power Systems

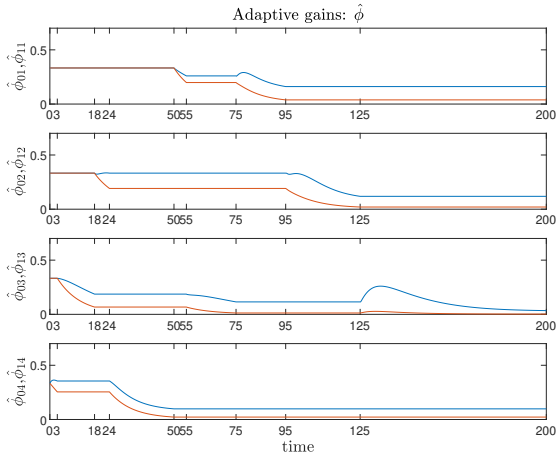

Figure 7. Adaptive gains $\hat{\phi}_{0p}$ (blue line) and $\hat{\phi}_{1p}$ (red line) for each topology.

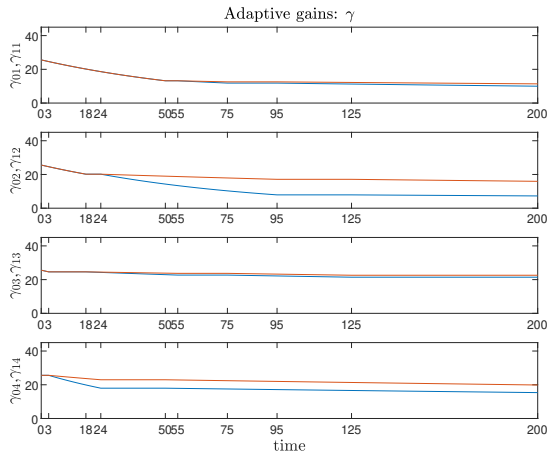

Figure 8. Adaptive gains $\hat{\gamma}_{0p}$ (blue line) and $\hat{\gamma}_{1p}$ (red line) for each topology.

active intervals, respectively. Utilizing these observations and the upper bound structure (14) of uncertainty, (21) becomes

$$\begin{aligned}\dot{V}(t) \leq & -\frac{1}{2}\boldsymbol{\xi}^T(t)\mathbf{Q}_{\sigma(t_{l+1}^-)}\boldsymbol{\xi}(t) \\ & - \left[(\hat{\phi}_{0\sigma}-\phi_{0\sigma}^*)+(\hat{\phi}_{1\sigma}-\phi_{1\sigma}^*)\|\boldsymbol{\xi}\|\right]\|\mathbf{r}_{\sigma(t_{l+1}^-)}\| \\ & + \sum_{i=0,p=\sigma(t_{l+1}^-)}^{1}(\hat{\phi}_{ip}(t)-\phi_{ip}^*)\dot{\hat{\phi}}_{ip}(t) + \sum_{\overline{p}\in\mathcal{I}(p)}\sum_{i=0}^{1}\gamma_{i\overline{p}}(t)\dot{\gamma}_{i\overline{p}}(t). \quad (23)\end{aligned}$$

Using the adaptive law (16a) we have for $p=\sigma(t_{l+1}^-)$

$$\begin{aligned}&\sum_{i=0,p=\sigma(t_{l+1}^-)}^{1}(\hat{\phi}_{ip}-\phi_{ip}^*)\dot{\hat{\phi}}_{ip} \\ &\quad = \left[(\hat{\phi}_{0\sigma}-\phi_{0\sigma}^*)+(\hat{\phi}_{1\sigma}-\phi_{1\sigma}^*)\|\boldsymbol{\xi}\|\right]\|\mathbf{r}_p\| \\ &\quad + \sum_{i=0,p=\sigma(t_{l+1}^-)}^{1}\left\{\alpha_{ip}\hat{\phi}_{ip}\phi_{ip}^* - \alpha_{ip}\hat{\phi}_{ip}^2\right\}. \quad (24)\end{aligned}$$

Similarly, the adaptive law (16b) leads to

$$\gamma_{i\overline{p}}\dot{\gamma}_{i\overline{p}} = -\left(\beta_{i\overline{p}}+\overline{\nu}_{i\overline{p}}\hat{\phi}_{i\overline{p}}^4\right)\gamma_{i\overline{p}}^2 + \beta_{i\overline{p}}\nu_{i\overline{p}}\gamma_{i\overline{p}}. \quad (25)$$

Investigating the adaptive laws (16a)-(16b) and the initial gain conditions (16c), it can be verified that there exists a positive fixed scalar $\underline{\gamma}_{i\overline{p}}$such that

$$\hat{\phi}_{ip}(t)\geq 0 \text{ and } \gamma_{i\overline{p}}(t)\geq \underline{\gamma}_{i\overline{p}} > 0 \quad \forall t\geq 0. \quad (26)$$

From (26) we have $\gamma_{i\overline{p}}\geq \underline{\gamma}_{i\overline{p}} \quad \forall t\geq 0$. Applying this relation to the second term of (25) yields

$$\gamma_{i\overline{p}}\dot{\gamma}_{i\overline{p}} \leq -\beta_{i\overline{p}}\gamma_{i\overline{p}}^2 - \underline{\gamma}_{i\overline{p}}^2\overline{\nu}_{i\overline{p}}\hat{\phi}_{i\overline{p}}^4 + \beta_{i\overline{p}}\nu_{i\overline{p}}\gamma_{i\overline{p}}. \quad (27)$$

The following simplification can be made

$$\begin{aligned}&-\underline{\gamma}_{i\overline{p}}^2\overline{\nu}_{i\overline{p}}\hat{\phi}_{i\overline{p}}^4 + \frac{\zeta_p}{2}\hat{\phi}_{i\overline{p}}^2 = -\underline{\gamma}_{i\overline{p}}^2\overline{\nu}_{i\overline{p}}\left(\hat{\phi}_{i\overline{p}}^4 - 2\hat{\phi}_{ip}^2\cdot\frac{\zeta_p}{4\underline{\gamma}_{i\overline{p}}^2\overline{\nu}_{i\overline{p}}}\right) \\ &= -\underline{\gamma}_{i\overline{p}}^2\overline{\nu}_{i\overline{p}}\left(\hat{\phi}_{i\overline{p}}^2 - \frac{\zeta_p}{4\underline{\gamma}_{i\overline{p}}^2\overline{\nu}_{i\overline{p}}}\right)^2 + \frac{\zeta_p^2}{16\underline{\gamma}_{i\overline{p}}^2\overline{\nu}_{i\overline{p}}}. \quad (28)\end{aligned}$$

Substituting (24), (27) and (28) in (23) yields

$$\begin{aligned}\dot{V}(t) \leq & -\frac{1}{2}\lambda_{\min}(\mathbf{Q}_{\sigma(t_{l+1}^-)})\|\boldsymbol{\xi}(t)\|^2 + \sum_{i=0,\ p=\sigma(t_{l+1}^-)}^{1}\Big(\alpha_{ip}\hat{\phi}_{ip}(t)\phi_{ip}^* \\ & - \alpha_{ip}\hat{\phi}_{ip}^2(t)\Big) + \sum_{\overline{p}\in\mathcal{I}(p)}\sum_{i=0}^{1}\Big(\beta_{i\overline{p}}\nu_{i\overline{p}}\gamma_{i\overline{p}} - \beta_{i\overline{p}}\gamma_{i\overline{p}}^2 - \frac{\zeta_p}{2}\hat{\phi}_{i\overline{p}}^2 \\ & + \frac{\zeta_p^2}{16\underline{\gamma}_{i\overline{p}}^2\overline{\nu}_{i\overline{p}}}\Big). \quad (29)\end{aligned}$$

Since $\hat{\phi}_{ip}\geq 0$ by (26), the Lyapunov function (18) yields

$$V \leq \frac{1}{2}\lambda_{\max}(\mathbf{P}_\sigma)\|\boldsymbol{\xi}\|^2 + \frac{1}{2}\sum_{p=1}^{N}\sum_{i=0}^{1}(\hat{\phi}_{ip}^2 + {\phi_{ip}^*}^2 + \gamma_{ip}^2). \quad (30)$$

From the definitions of $\zeta, \zeta_p, \alpha_{ip}, \beta_{i\overline{p}}$ and using (30), the condition (29) is further simplified to

$$\begin{aligned}\dot{V}(t) \leq & -\zeta V(t) + \sum_{i=0,\ p=\sigma(t_{l+1}^-)}^{1}\Big(\alpha_{ip}\hat{\phi}_{ip}(t)\phi_{ip}^* - \bar{\alpha}_{ip}\hat{\phi}_{ip}^2(t) + \frac{\zeta_p}{2}\gamma_{ip}^2\Big) \\ & + \sum_{p=1}^{N}\sum_{i=0}^{1}\frac{\zeta_p}{2}{\phi_{ip}^*}^2 + \sum_{\overline{p}\in\mathcal{I}(p)}\sum_{i=0}^{1}\Big(\beta_{i\overline{p}}\nu_{i\overline{p}}\gamma_{i\overline{p}}(t) - \bar{\beta}_{i\overline{p}}\gamma_{i\overline{p}}^2(t) \\ & + \frac{\zeta_p^2}{16\underline{\gamma}_{i\overline{p}}^2\overline{\nu}_{i\overline{p}}}\Big) \quad (31)\end{aligned}$$

where $\bar{\alpha}_{ip}\triangleq(\alpha_{ip}-\frac{\zeta_p}{2})>0$ and $\bar{\beta}_{i\overline{p}}\triangleq(\beta_{i\overline{p}}-\frac{\zeta_{\overline{p}}}{2})>0$. Again, the following simplification is made

$$\alpha_{ip}\hat{\phi}_{ip}\phi_{ip}^* - \bar{\alpha}_{ip}\hat{\phi}_{ip}^2 = -\bar{\alpha}_{ip}\left(\hat{\phi}_{ip} - \frac{\alpha_{ip}\phi_{ip}^*}{2\bar{\alpha}_{ip}}\right)^2 + \frac{\left(\alpha_{ip}\phi_{ip}^*\right)^2}{4\bar{\alpha}_{ip}}. \quad (32)$$

It can be noted from the adaptive laws (16) that $\gamma_{i\overline{p}}$ decreases for the inactive systems and remains unchanged for the active one. Coupled with the fact $\gamma_{ip}\geq\underline{\gamma}_{ip} \quad \forall t\geq 0$, it is concluded that $\gamma_{ip}\in\mathcal{L}_\infty \ \forall p\in\Omega$. Then $\exists\bar{\gamma}_{ip}\in\mathbb{R}^+$ such that $\gamma_{ip}(t)\leq\bar{\gamma}_{ip}$. Using $0<\kappa<\zeta$, (32), $\dot{V}(t)$ in (31) simplifies to

$$\dot{V}(t) \leq -\kappa V(t) - (\zeta-\kappa)V(t) + \varsigma + \varsigma_2, \quad (33)$$

where $\varsigma \triangleq \sum_{p=1}^{N}\sum_{i=0}^{1}\frac{\zeta_p}{2}{\phi_{ip}^*}^2+\sum_{\overline{p}\in\mathcal{I}(p)}\sum_{i=0}^{1}\left(\beta_{ip}\nu_{i\overline{p}}\bar{\gamma}_{ip}+(\zeta_p^2/(16\overline{\nu}_{i\overline{p}}\underline{\gamma}_{i\overline{p}}^2)\right)$ and $\varsigma_2 \triangleq \sum_{i=0,p=\sigma(t_{l+1}^-)}^{1}\frac{\left(\alpha_{ip}\phi_{ip}^*\right)^2}{4\bar{\alpha}_{ip}}+\frac{\zeta_p}{2}\bar{\gamma}_{ip}^2$.

Scenario $S2$**:** In this scenario we have $\|\mathbf{r}_\sigma\|<\varphi$. Therefore,

$$\begin{aligned}\dot{V}(t)\leq&-(1/2)\boldsymbol{\xi}^T(t)\mathbf{Q}_{\sigma(t_{l+1}^-)}\boldsymbol{\xi}(t)\\&-(1-\bar{J})\rho_{\sigma(t_{l+1}^-)}\omega\frac{\|\mathbf{r}_{\sigma(t_{l+1}^-)}\|^2}{\sqrt{\|\mathbf{r}_{\sigma(t_{l+1}^-)}\|^2+\epsilon}}\\&+\left[\phi_{0\sigma}^*+\phi_{1\sigma}^*\|\boldsymbol{\xi}\|\right]\|\mathbf{r}_{\sigma(t_{l+1}^-)}\|\\&\sum_{i=0,p=\sigma(t_{l+1}^-)}^{1}(\hat{\phi}_{ip}(t)-\phi_{ip}^*)\dot{\hat{\phi}}_{ip}(t)+\sum_{\overline{p}\in\mathcal{I}(p)}\sum_{i=0}^{1}\gamma_{i\overline{p}}(t)\dot{\gamma}_{i\overline{p}}(t)\\\leq&-\frac{1}{2}\boldsymbol{\xi}^T(t)\mathbf{Q}_{\sigma(t_{l+1}^-)}\boldsymbol{\xi}(t)+\left[\phi_{0\sigma}^*+\phi_{1\sigma}^*\|\boldsymbol{\xi}\|\right]\|\mathbf{r}_{\sigma(t_{l+1}^-)}\|\\&\sum_{i=0,p=\sigma(t_{l+1}^-)}^{1}(\hat{\phi}_{ip}(t)-\phi_{ip}^*)\dot{\hat{\phi}}_{ip}(t)+\sum_{\overline{p}\in\mathcal{I}(p)}\sum_{i=0}^{1}\gamma_{i\overline{p}}(t)\dot{\gamma}_{i\overline{p}}(t).\end{aligned}\tag{34}$$

Then, following similar lines as in Scenario $S1$, we have

$$\begin{aligned}\dot{V}(t)\leq&-\kappa V(t)-(\zeta-\kappa)V(t)+\left[\hat{\phi}_{0\sigma}+\hat{\phi}_{1\sigma}\|\boldsymbol{\xi}\|\right]\|\mathbf{r}_{\sigma(t_{l+1}^-)}\|\\&+\varsigma+\varsigma_2,\end{aligned}\tag{35}$$

From (10) one has $\|\mathbf{r}\|<\varphi\Rightarrow\|\boldsymbol{\xi}\|\in\mathcal{L}_\infty$ and consequently, the adaptive law (16a) implies $\|\mathbf{r}\|,\|\boldsymbol{\xi}\|\in\mathcal{L}_\infty\Rightarrow\dot{\hat{\phi}}_{ip}(t)\in\mathcal{L}_\infty$. Therefore, $\exists\varsigma_1\in\mathbb{R}^+$ such that $\mathbf{Y}^T\hat{\mathbf{\Phi}}_p\leq\varsigma_1,\forall\sigma\in\Omega$ when $\|\mathbf{r}_\sigma\|<\varphi$. Hence, replacing this relation in (35) yields

$$\dot{V}(t)\leq-\kappa V(t)-(\zeta-\kappa)V(t)+\varphi\varsigma_1+\varsigma+\varsigma_2.\tag{36}$$

Further, combining (33) and (36) we define the scalar

$$\mathcal{B}\triangleq\frac{\varphi\varsigma_1+\varsigma+\varsigma_2}{(\zeta-\kappa)}.\tag{37}$$

From the two scenarios $S1$ and $S2$, it can be concluded that $\dot{V}(t)\leq-\kappa V(t)$ when $V(t)\geq\mathcal{B}$. In light of this, further analysis is needed to observe the behavior of $V(t)$

- **(i)** when $V(t)\geq\mathcal{B}$, we have $\dot{V}(t)\leq-\kappa V(t)$ from (33) implying exponential decrease of $V(t)$;
- **(ii)** when $V(t)<\mathcal{B}$, $V(t)$ may increase.

Such behavior can be analyzed along the lines of [45], [47], and eventually leads to the bound

$$V(t)\leq\max\left\{cV(0),c\mu\mathcal{B}\right\},\quad\forall t\geq0.\tag{38}$$

Again, the definition of the Lyapunov function (18) yields

$$V(t)\geq(1/2)\lambda_{\min}(\mathbf{P}_{\sigma(t)})\|\boldsymbol{\xi}\|^2\geq(\underline{\zeta}_m/2)\|\boldsymbol{\xi}\|^2.\tag{39}$$

Using (38) and (39) we have

$$\|\boldsymbol{\xi}\|^2\leq(2/\underline{\zeta}_m)\max\left\{cV(0),c\mu\mathcal{B}\right\},\quad\forall t\geq0.\tag{40}$$

Therefore, using the expression of $\mathcal{B}$ from (30), an ultimate bound b on the tracking error $\boldsymbol{\xi}$ can be found as

$$b=\sqrt{\frac{2\bar{\zeta}_M^{(N_0+1)}\left(\varphi\varsigma_1+\varsigma+\varsigma_2\right)}{\underline{\zeta}_m^{(N_0+2)}\left(\zeta-\kappa\right)}}\tag{41}$$

REFERENCES

[1] C. Zhao, U. Topcu, N. Li, and S. Low, "Design and stability of load-side primary frequency control in power systems," *IEEE Transactions on Automatic Control*, vol. 59, no. 5, pp. 1177–1189, 2014.

[2] S. Ghosh, K. A. Folly, and A. Patel, "Synchronized versus non-synchronized feedback for speed-based wide-area PSS: Effect of time-delay," *IEEE Transactions on Smart Grid*, vol. 9, no. 5, pp. 3976–3985, 2018.

[3] S. Saxena and Y. V. Hote, "Load frequency control in power systems via internal model control scheme and model-order reduction," *IEEE Transactions on Power Systems*, vol. 28, no. 3, pp. 2749–2757, 2013.

[4] A. M. Ersdal, L. Imsland, and K. Uhlen, "Model predictive load-frequency control," *IEEE Transactions on Power Systems*, vol. 31, no. 1, pp. 777–785, 2016.

[5] E. Mallada, C. Zhao, and S. Low, "Optimal load-side control for frequency regulation in smart grids," *IEEE Transactions on Automatic Control*, vol. 62, no. 12, pp. 6294–6309, 2017.

[6] S. Sönmez and S. Ayasun, "Stability region in the parameter space of pi controller for a single-area load frequency control system with time delay," *IEEE Transactions on Power Systems*, vol. 31, no. 1, pp. 829–830, 2015.

[7] R. Dey, S. Ghosh, G. Ray, and A. Rakshit, "$\mathcal{H}_\infty$ load frequency control of interconnected power systems with communication delays," *International Journal of Electrical Power & Energy Systems*, vol. 42, no. 1, pp. 672 – 684, 2012.

[8] X. Wang, Y. Wang, and Y. Liu, "Dynamic load frequency control for high-penetration wind power considering wind turbine fatigue load," *International Journal of Electrical Power Energy Systems*, vol. 117, p. 105696, 2020.

[9] X. Shang-Guan, Y. He, C. Zhang, L. Jiang, J. W. Spencer, and M. Wu, "Sampled-data based discrete and fast load frequency control for power systems with wind power," *Applied Energy*, vol. 259, p. 114202, 2020.

[10] S. A. Hosseini, M. Toulabi, A. S. Dobakhshari, A. Ashouri-Zadeh, and A. M. Ranjbar, "Delay compensation of demand response and adaptive disturbance rejection applied to power system frequency control," *IEEE Transactions on Power Systems*, vol. 35, no. 3, pp. 2037–2046, 2020.

[11] B. Sonker, D. Kumar, and P. Samuel, "Dual loop IMC structure for load frequency control issue of multi-area multi-sources power systems," *International Journal of Electrical Power Energy Systems*, vol. 112, pp. 476 – 494, 2019.

[12] P. Babahajiani, Q. Shafiee, and H. Bevrani, "Intelligent demand response contribution in frequency control of multi-area power systems," *IEEE Transactions on Smart Grid*, vol. 9, no. 2, pp. 1282–1291, 2018.

[13] A. Ameli, A. Hooshyar, E. F. El-Saadany, and A. M. Youssef, "Attack detection and identification for automatic generation control systems," *IEEE Transactions on Power Systems*, vol. 33, no. 5, pp. 4760–4774, 2018.

[14] L. Fan, Z. Miao, and D. Osborn, "Wind farms with hvdc delivery in load frequency control," *IEEE Transactions on Power Systems*, vol. 24, no. 4, pp. 1894–1895, 2009.

[15] A. Abazari, H. Monsef, and B. Wu, "Coordination strategies of distributed energy resources including FESS, DEG, FC and WTG in load frequency control (LFC) scheme of hybrid isolated micro-grid," *International Journal of Electrical Power & Energy Systems*, vol. 109, pp. 535 – 547, 2019.

[16] C. D. Korkas, S. Baldi, I. Michailidis, and E. B. Kosmatopoulos, "Occupancy-based demand response and thermal comfort optimization in microgrids with renewable energy sources and energy storage," *Applied Energy*, vol. 163, pp. 93 – 104, 2016.

[17] C. Pan and C. Liaw, "An adaptive controller for power system load-frequency control," *IEEE Transactions on Power Systems*, vol. 4, no. 1, pp. 122–128, 1989.

[18] S. Hanwate, Y. V. Hote, and S. Saxena, "Adaptive policy for load frequency control," *IEEE Transactions on Power Systems*, vol. 33, no. 1, pp. 1142–1144, 2018.

[19] B. Polajžer, M. Petrun, and J. Ritonja, "Adaptation of load-frequency-control target values based on the covariances between area-control errors," *IEEE Transactions on Power Systems*, vol. 33, no. 6, pp. 5865–5874, 2018.

[20] C. Boonchuay, "Improving regulation service based on adaptive load frequency control in lmp energy market," *IEEE Transactions on Power Systems*, vol. 29, no. 2, pp. 988–989, 2014.

[21] A. M. Prostejovsky, M. Marinelli, M. Rezkalla, M. H. Syed, and E. Guillo-Sansano, "Tuningless load frequency control through active engagement of distributed resources," *IEEE Transactions on Power Systems*, vol. 33, no. 3, pp. 2929–2939, 2018.

[22] C. Li, Y. Wu, Y. Sun, H. Zhang, Y. Liu, Y. Liu, and V. Terzija, "Continuous under-frequency load shedding scheme for power system adaptive frequency control," *IEEE Transactions on Power Systems*, vol. 35, no. 2, pp. 950–961, 2020.

[23] X. Zhao-xia, Z. Mingke, H. Yu, J. M. Guerrero, and J. C. Vasquez, "Coordinated primary and secondary frequency support between microgrid and weak grid," *IEEE Transactions on Sustainable Energy*, vol. 10, no. 4, pp. 1718–1730, 2019.

[24] T. Liu, D. J. Hill, and C. Zhang, "Non-disruptive load-side control for frequency regulation in power systems," *IEEE Transactions on Smart Grid*, vol. 7, no. 4, pp. 2142–2153, 2016.

[25] Y. Han, H. Li, P. Shen, E. A. A. Coelho, and J. M. Guerrero, "Review of active and reactive power sharing strategies in hierarchical controlled microgrids," *IEEE Transactions on Power Electronics*, vol. 32, no. 3, pp. 2427–2451, 2017.

[26] C. Zhang, T. Liu, and D. J. Hill, "Switched distributed load-side frequency control of power systems," *International Journal of Electrical Power & Energy Systems*, vol. 105, pp. 709 – 716, 2019.

[27] H. A. Yousef, K. AL-Kharusi, M. H. Albadi, and N. Hosseinzadeh, "Load frequency control of a multi-area power system: An adaptive fuzzy logic approach," *IEEE Transactions on Power Systems*, vol. 29, no. 4, pp. 1822–1830, 2014.

[28] A. Sargolzaei, K. K. Yen, and M. N. Abdelghani, "Preventing time-delay switch attack on load frequency control in distributed power systems," *IEEE Transactions on Smart Grid*, vol. 7, no. 2, pp. 1176–1185, 2016.

[29] Y. Wu, Z. Wei, J. Weng, X. Li, and R. H. Deng, "Resonance attacks on load frequency control of smart grids," *IEEE Transactions on Smart Grid*, vol. 9, no. 5, pp. 4490–4502, 2018.

[30] S. Alhalali, C. Nielsen, and R. El-Shatshat, "Mitigation of cyber-physical attacks in multi-area automatic generation control," *International Journal of Electrical Power & Energy Systems*, vol. 112, pp. 362–369, 2019.

[31] M. S. Mahmoud, M. M. Hamdan, and U. A. Baroudi, "Modeling and control of cyber-physical systems subject to cyber attacks: A survey of recent advances and challenges," *Neurocomputing*, vol. 338, pp. 101 – 115, 2019.

[32] C. Peng, J. Li, and M. Fei, "Resilient event-triggering H_∞ load frequency control for multi-area power systems with energy-limited DoS attacks," *IEEE Transactions on Power Systems*, vol. 32, no. 5, pp. 4110–4118, 2017.

[33] J. Schiffer, F. Dorfler, and E. Fridman, "Robustness of distributed averaging control in power systems: Time delays & dynamic communication topology," *Automatica*, vol. 80, pp. 261 – 271, 2017.

[34] L. Vu and D. Liberzon, "Supervisory control of uncertain linear time-varying systems," *IEEE Transactions on Automatic Control*, vol. 56, no. 1, pp. 27–42, 2011.

[35] B. Niu, P. Zhao, J.-D. Liu, H.-J. Ma, and Y.-J. Liu, "Global adaptive control of switched uncertain nonlinear systems: An improved MDADT method," *Automatica*, vol. 115, p. 108872, 2020.

[36] X. Jin, W. M. Haddad, and T. Yucelen, "An adaptive control architecture for mitigating sensor and actuator attacks in cyber-physical systems," *IEEE Transactions on Automatic Control*, vol. 62, no. 11, pp. 6058–6064, 2017.

[37] S. Yuan, L. Li, B. Cai, and L. Zhang, "Differential Riccati equation-based adaptive stabilization for switched linear systems," *International Journal of Robust and Nonlinear Control*, vol. 30, no. 1, pp. 51–64, 2020.

[38] L. An and G. Yang, "Decentralized adaptive fuzzy secure control for nonlinear uncertain interconnected systems against intermittent DoS attacks," *IEEE Transactions on Cybernetics*, vol. 49, no. 3, pp. 827–838, 2019.

[39] J. Giraldo, E. Mojica-Nava, and N. Quijano, "Synchronisation of heterogeneous kuramoto oscillators with sampled information and a constant leader," *International Journal of Control*, vol. 92, no. 11, pp. 2591–2607, 2019.

[40] F. Dorfler and F. Bullo, "Synchronization and transient stability in power networks and nonuniform Kuramoto oscillators," *SIAM Journal on Control and Optimization*, vol. 50, no. 3, pp. 1616–1642, 2012.

[41] S. Trip and C. De Persis, "Distributed optimal load frequency control with non-passive dynamics," *IEEE Transactions on Control of Network Systems*, vol. 5, no. 3, pp. 1232–1244, 2018.

[42] J. W. Simpson-Porco, F. Dorfler, and F. Bullo, "Synchronization and power sharing for droop-controlled inverters in islanded microgrids," *Automatica*, vol. 49, no. 9, pp. 2603 – 2611, 2013.

[43] S. Baldi, T. Tao, and E. B. Kosmatopoulos, "Adaptive hybrid synchronisation in uncertain Kuramoto networks with limited information," *IET Control Theory Applications*, vol. 13, no. 9, pp. 1229–1238, 2019.

[44] R. Ortega, A. Loria, P. J. Nicklasson, and H. Sira-Ramirez, *Passivity-based Control of Euler-Lagrange Systems*. Springer, 2008.

[45] S. Roy and S. Baldi, "A simultaneous adaptation law for a class of nonlinearly parametrized switched systems," *IEEE Control Systems Letters*, vol. 3, no. 3, pp. 487–492, 2019.

[46] J. J. Grainger and W. D. Stevenson, *Power system analysis*. McGraw-Hill, 1994.

[47] J. P. Hespanha and A. S. Morse, "Stability of switched systems with average dwell-time," in *Proceedings of the 38th IEEE Conference on Decision and Control*, vol. 3. IEEE, 1999, pp. 2655–2660.

[48] F. Dorfler and F. Bullo, "Synchronization and transient stability in power networks and nonuniform Kuramoto oscillators," *SIAM Journal on Control and Optimization*, vol. 50, no. 3, pp. 1616–1642, 2012.

[49] V. Utkin, J. Guldner, and J. Shi, *Sliding mode control in electromechanical systems*. CRC Press, 2009.

[50] K. Vrdoljak, N. Perić, and I. Petrović, "Sliding mode based load-frequency control in power systems," *Electric Power Systems Research*, vol. 80, no. 5, pp. 514 – 527, 2010.

[51] Y. Shtessel, M. Taleb, and F. Plestan, "A novel adaptive-gain supertwisting sliding mode controller: Methodology and application," *Automatica*, vol. 48, no. 5, pp. 759–769, 2012.

[52] P. A. Ioannou and J. Sun, *Robust adaptive control*. Courier Corporation, 2012.

[53] A. Moeini, I. Kamwa, P. Brunelle, and G. Sybille, "Open data IEEE test systems implemented in SimPowerSystems for education and research in power grid dynamics and control," in *2015 50th International Universities Power Engineering Conference (UPEC)*, 2015, pp. 1–6.

Tian Tao received her B.S. degree in department of Electrical Engineering Automation from Wuhan Polytechnic University, Wuhan, China in 2013, M.S. degree in Automation Engineering department from University of Electronic Science and Technology of China, Sichuan in 2018. She is currently pursuing the PhD in Systems and Control at Delft University of Technology (TU Delft), The Netherlands. Her research interests are adaptive switched control with applications in networked systems.

Spandan Roy received the B.Tech. in electronics and communication engineering from Techno India (Salt Lake), West Bengal University of Technology, Kolkata, India, in 2011, the M.Tech. in mechatronics from Academy of Scientific and Innovative Research, New Delhi, India, in 2013, and the Ph.D. in control and automation from Indian Institute of Technology Delhi, India, in 2018. He is currently Assistant Professor with Robotics Research Center, International Institute of Information Technology Hyderabad, India. Previously, he was Postdoc Researcher with Delft Center for System and Control, TU Delft, The Netherlands. His research interests include artificial delay based control, adaptive-robust control, switched systems and its applications in Euler-Lagrange systems.

Simone Baldi (M'14, SM'19) received the B.Sc. in electrical engineering, and the M.Sc. and Ph.D. in automatic control engineering from University of Florence, Italy, in 2005, 2007, and 2011. He is professor at School of Mathematics and School of Cyber Science and Engineering, Southeast University, with guest position at Delft Center for Systems and Control, TU Delft, where he was assistant professor. He was awarded outstanding reviewer for *Applied Energy* (2016) and *Automatica* (2017). He is subject editor of *Int. Journal of Adaptive Control and Signal Processing*. His research interests are adaptive and learning systems with applications in unmanned vehicles and smart energy systems.